

CAAP Quarterly Report

Date of Report: <July 10th, 2017>

Contract Number: <DTPH56-15-H-CAAP06>

Prepared for: <Government Agency: U. S. DOT PHMSA >

Project Title: <Mitigating Pipeline Corrosion Using A Smart Thermal Spraying Coating System>

Prepared by: <North Dakota State University>

Contact Information: <Dr. Fardad Azarmi, Email: fardad.azarmi@ndsu.edu, Phone: 701.231.9784; Dr. Ying Huang, Email: ying.huang@ndsu.edu, Phone: 701.231.7651.>

For quarterly period ending: <July 10th, 2017>

Business and Activity Section

(a) Generated Commitments

No changes to the existing agreement.

No equipment purchased over this reporting period.

No supplies purchased in this quarter.

(b) Status Update of Past Quarter Activities

Studies were conducted during this quarter by comparison of microstructural characteristics of recently developed Al-Zn wire arc sprayed coating with some previously developed coatings in this project before and after corrosion test (Task 2 Subtask 2.3 & 2.4). The work also continued with a comprehensive analyze of the corrosion status of laboratory tested samples with soft coatings for quantitative corrosion assessment using embedded fiber optic sensors (Task 3 Subtask 3.2): 1) experimental setup; 2) experimental data; and 3) data analysis and comparison between soft and hard coatings. Further efforts will be focused on more material analysis on coatings, corrosion tests on coating samples with embedded sensors in hard coatings and duplex coatings, and comparison of the different corrosion performance of the coatings toward corrosion. The detail progresses, which were completed in this quarter, are presented below:

1) Microstructural characterization of the Al-Zn coating deposited by wire arc spraying technology and other thermal sprayed metallic coatings before and after corrosion tests (Task 2 Subtask 2.3 & 2.4)- Continued from the previous report.

The aim of this study was to better understand the effectiveness of the thermal sprayed coatings in term of corrosion behavior and also blocking the deleterious elements such as Cl⁻ to penetrate into the interior layers of the coatings. To this end, the coatings were subjected to the microstructural characterization techniques such as Scanning Electron Microscopy (SEM) and Electron Diffraction Spectroscopy (EDS). The SEM was also equipped with a Nanotracer EDS detector with a NORVAR light-element window. The accelerating voltage used for EDS was 15 keV to investigate the elemental distribution of the coatings before and after corrosion.

For HVOF deposited Al-Bronze coatings which had been studied previously, the SEM micrographs taken from the cross-section of the coatings before and after corrosion were shown in Figure 1. It could be concluded that corrosion products significantly were formed on the surface of the HVOF deposited Al-bronze coating after corrosion (Figure 1). The dark gray areas presented very close to the surface of the coating were observed after corrosion which did not exist in the SEM micrograph of the HVOF deposited Al-bronze before corrosion. These areas could be associated to the corrosion products formed after exposing to the NaCl solution.

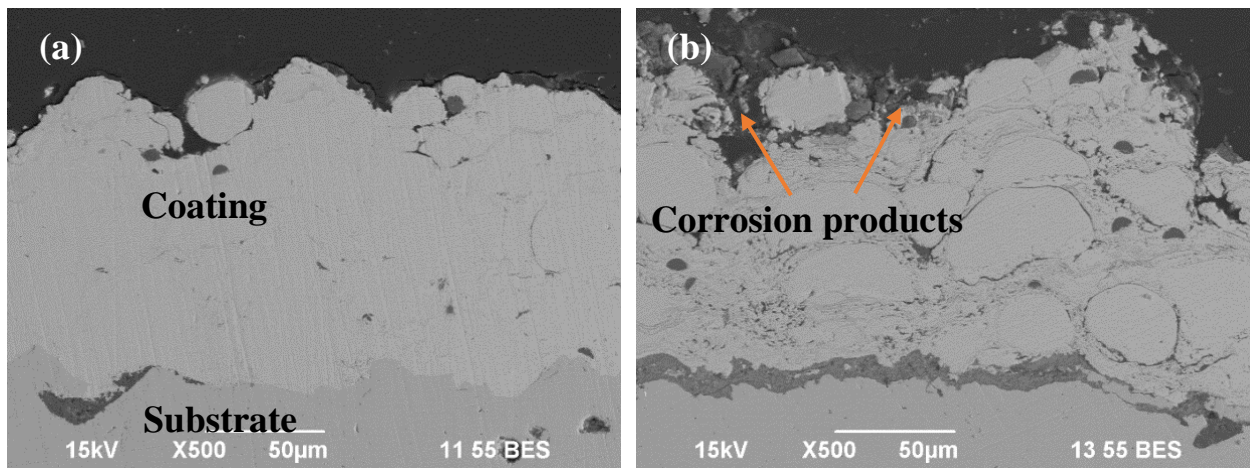


Figure 1. SEM micrographs of the HVOF deposited Al-bronze coating (a) before and (b) after corrosion.

Such corrosion products were not observed on the wire arc deposited Al-Zn as seen in Figures 2 (a, b) and Cu coatings as shown in Figures 2 (c, d). In fact, there was no observable change in the microstructure of the cross section of the coatings, preferably near the surface, before and after corrosion. It indicated very slim change (or if it happened in very small scale, less than few micrometers) in the composition of the Al-Zn and Copper coatings once exposed to the corrosive environment. Figure 2 (a-d) demonstrated this observations in the wire arc sprayed Al-Zn and Cu coatings.

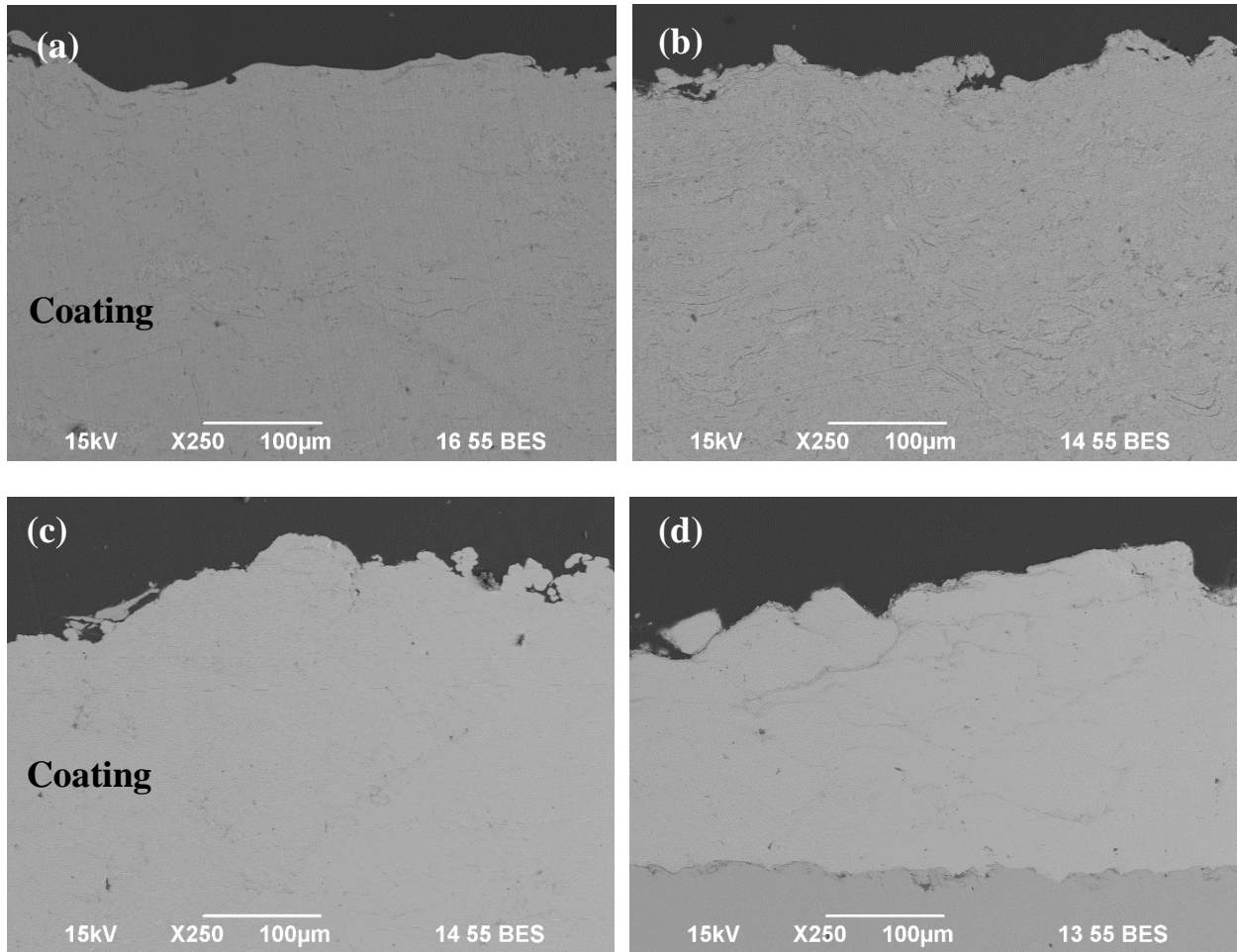


Figure 2. (a) Wire arc deposited Al-Zn coating before and (b) after corrosion, (c) HVOF deposited Copper coating before and (d) after corrosion.

The elemental distribution in the coatings' microstructures was studied by EDS mapping technique and were presented in Figure 3. The major objective of EDS mapping was to detect the depth of the penetration of the deletrious elements, preferably Cl^- , to estimate the effectiveness of the coating to act as a barrier to hinder diffusion of such a detrimenteous elements in to the coatings.

According to the EDS results, chlorine had diffused more in to HVOF deposited Al-Bronze compared to the two other coatings. That could be due to relatively high level of porosity detected in this coating. The other EDS map shown in Figure 4, demonstrated the penetration depth of the Na element inside the coatings. This value for the Al-Zn coating had the lowest value as it appeared as very small area which was overlapping with the Zn map. As could be seen from the images in figure 3, Al-bronze acted less effective compared to the other coatings in terms of blocking the sodium elements inside the coating.

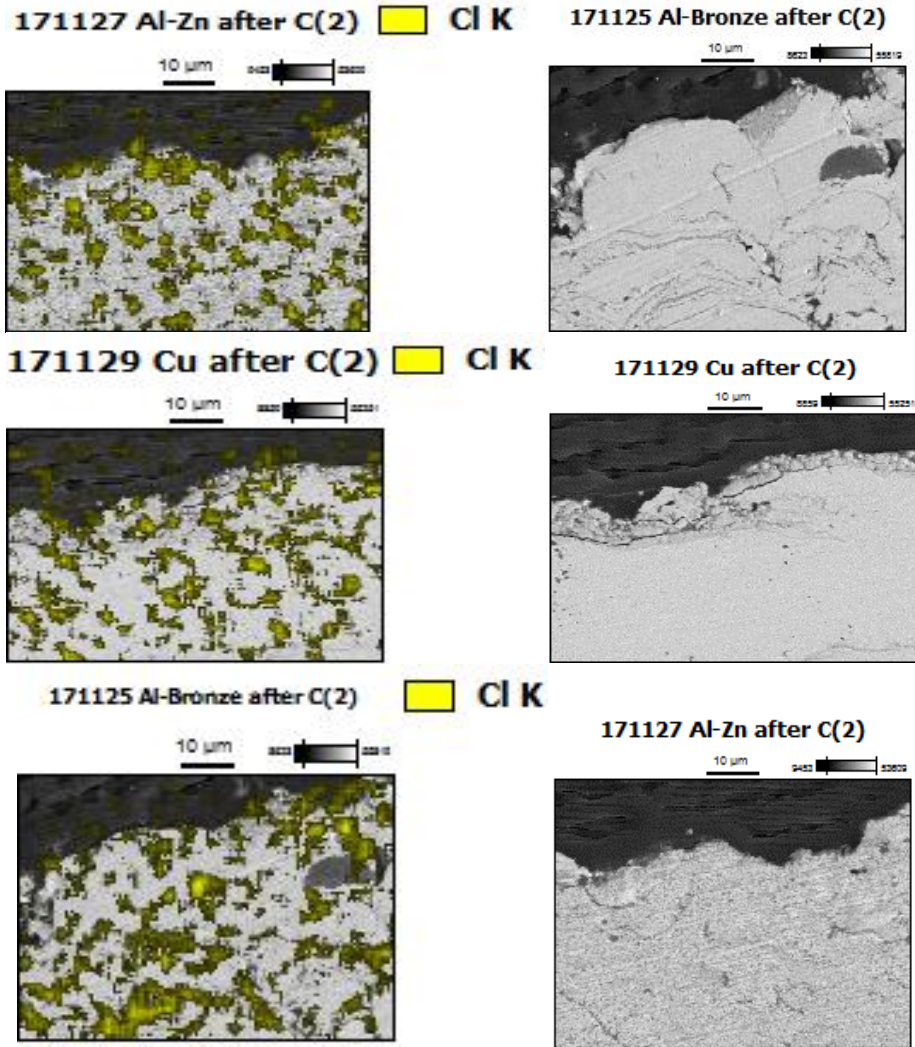


Figure 3. EDS maps of Cl⁻ element penetrated in a variety of thermally sprayed coatings after corrosion experiment in this project.

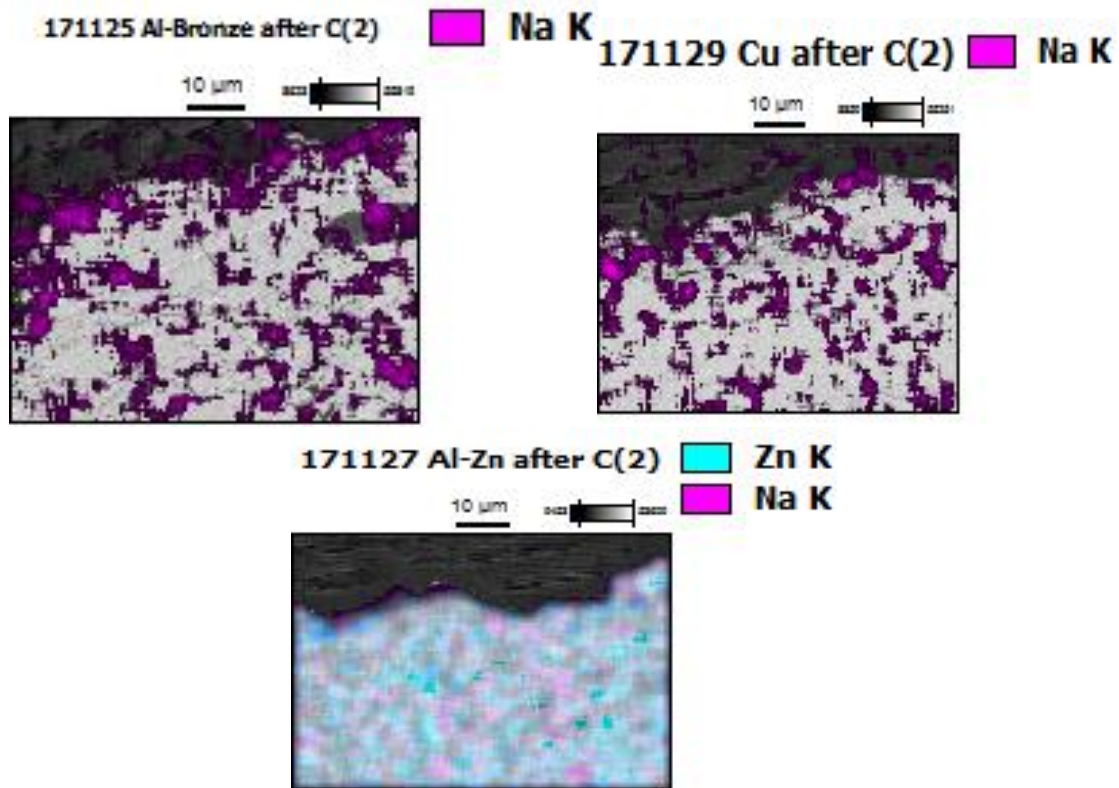


Figure 4. EDS maps of Na⁺ element penetrated in the thermal sprayed coatings.

The composition of the coatings before and after corrosion were also been evaluated by using a Rigaku Ultima IV diffractometer (Cu K α radiation, voltage 40 kV, current 44 mA, and a fixed incident angle of 1.5 degree in a parallel beam geometry).

After analyzing the XRD pattern of wire arc sprayed Al-Zn coating as shown in Figure 5, before corrosion, it was observed that the coating was mainly composed of Aluminum and Zinc. After corrosion, some other peaks belonged to aluminum oxide and zinc oxide detected, which were formed as the result of the passivation process of the surface. Presence of these oxides were also identified in the earlier report considering the Tafel curve obtained after corrosion of the Al-Zn coating in 3.5% NaCl solution.

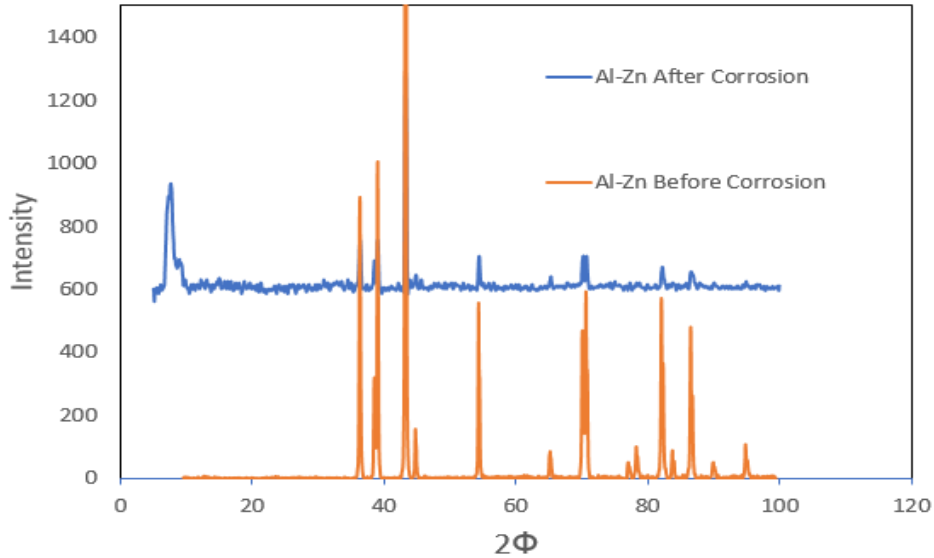


Figure 5. X-Ray pattern of wire arc sprayed Al-bronze coatings before and after corrosion.

XRD-pattern of the HVOF sprayed copper coatings which was also deposited earlier in this project exhibited some dissimilarity when comparing before and after corrosion conditions in this coating. The XRD pattern shown in Figure 6 demonstrated that copper oxide was the main composition appeared after corrosion whilst it was not detected in the coating structure before the corrosion experiments.

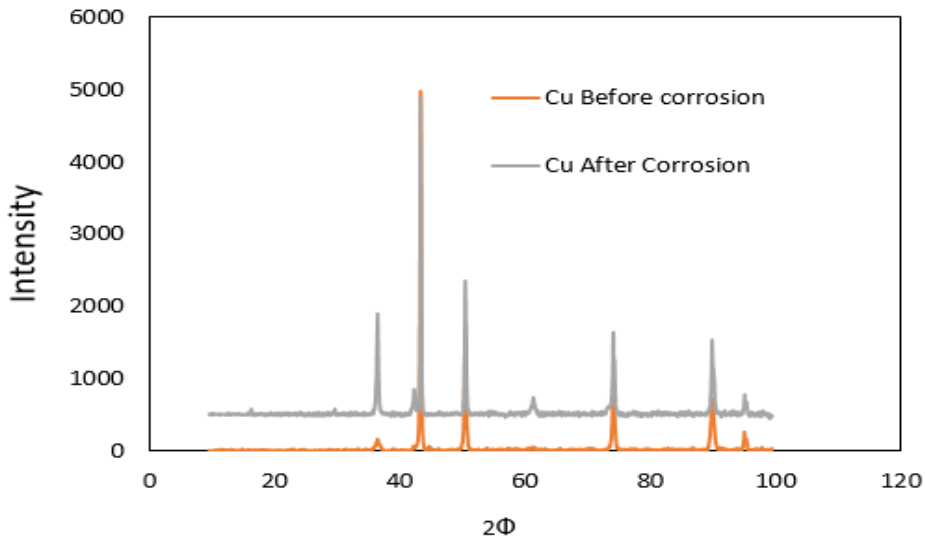


Figure 6. X-Ray pattern of HVOF sprayed Copper coatings before and after corrosion.

HVOF deposited Al-bronze was mainly contained $AlCu_3$ and $Ni_3ZnC_{0.7}$ before corrosion as it is shown in Figure 7. After exposed to the corrosive environment, there were more materials such as $AlCu_3$, Cu_2O , and $FeO(OH)$ were identified in the Al-bronze coating.

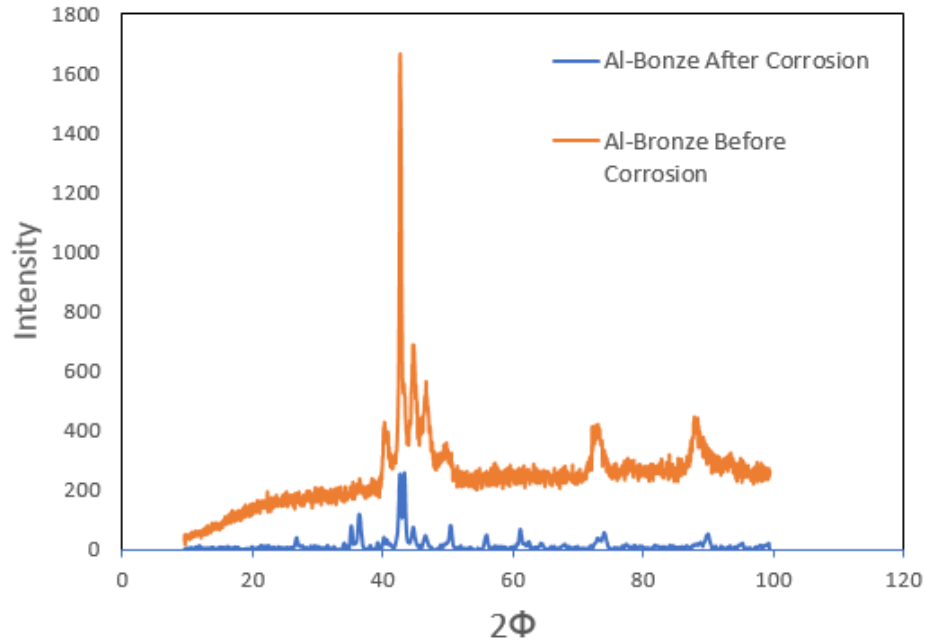


Figure 7. X-Ray pattern of HVOF sprayed Al-bronze coatings before and after corrosion.

All those experiments confirmed effectiveness of wire arc sprayed Al-Zn coating in corrosion prevention on steel substrate and its better quality compared to previously produced coatings in this study.

2) Experimental setup for quantitative corrosion assessment of soft coatings using embedded fiber optic sensors (Task 3 Subtask 3.2)

In the fifth quarterly report, it had been mentioned that long-term corrosion tests were carried on three steel plate samples with soft coatings. Epoxy (Duralco 4460 from Cotronics Corp.) had been used as soft coating in this case for the experiments. One optic fiber sensor was embedded on each sample beneath the soft coating to monitor the behavior of coating as time progressed. Figure 8 shows the three samples used in this experiment. The three samples plates (noted as Sample #S1, #S2, and #S3) were made of A36 structural steel and the thickness of soft coatings were 1mm. The corrosion tests run nine months by the time this quarterly report is drafted, resulting in 6,400 hours of monitoring time span. In addition to the three embedded sensors, one temperature compensation fiber optic sensor was placed on the sample to compensate the temperature effects on the corrosion monitoring.

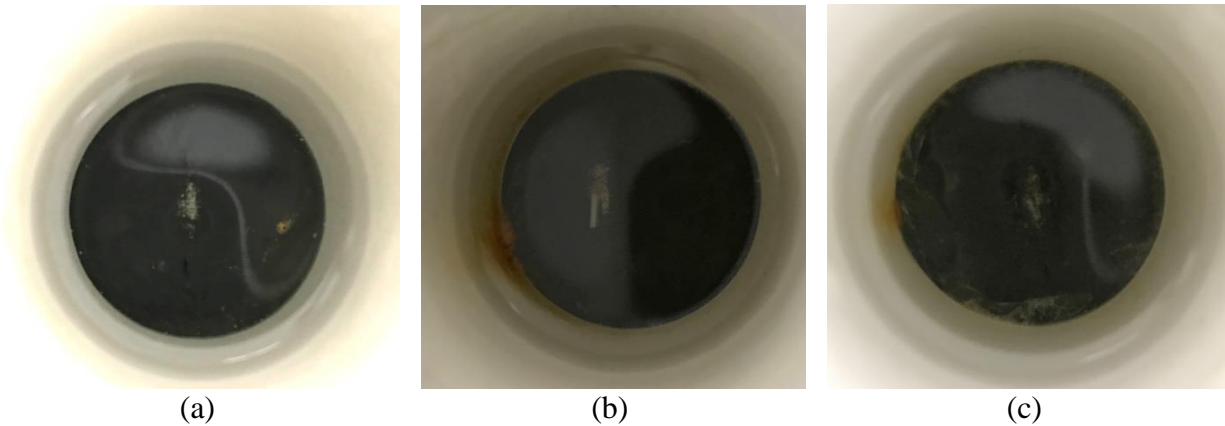


Figure 8. Visual inspection result at Day 1 for: (a) Sample #S1, (b) Sample #S2, and (c) Sample #S3.

3) Experimental data from embedded sensors in soft coatings (Task 3 Subtask 3.2)

Figure 9 shows the data collected from embedded corrosion monitoring system together with the data collected from the temperature compensation sensor. Figures 10 ~ 12 show the visual inspection results of all the samples on Day 30, Day 150, and Day 270.

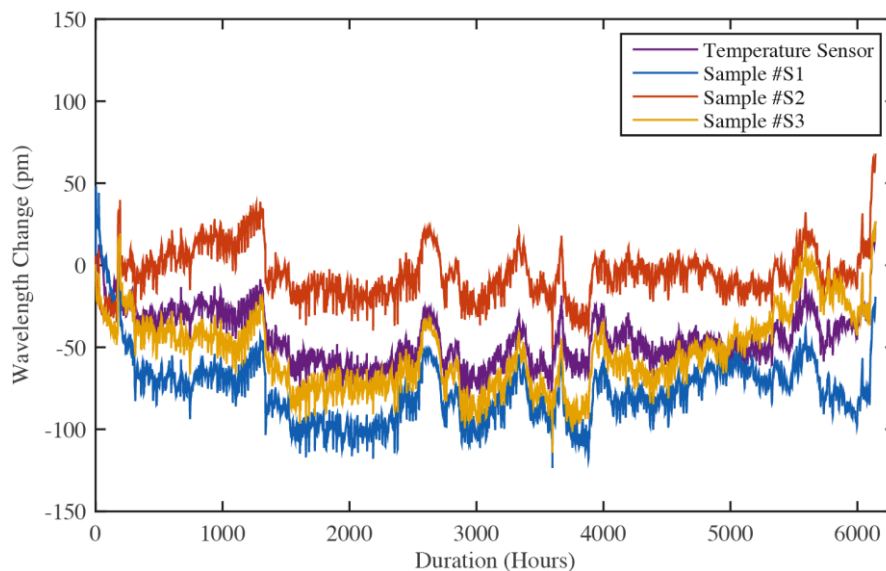


Figure 9. Bragg wavelength changes collected from FBG sensor without eliminating temperature effect and de-noising.



Figure 10. Visual inspection result at Day 30 for: (a) Sample #S1, (b) Sample #S2, and (c) Sample #S3.



Figure 11. Visual inspection result at Day 150 for: (a) Sample #S1, (b) Sample #S2, and (c) Sample #S3.



Figure 12. Visual inspection result at Day 270 (Jun 18th, 2017) for: (a) Sample #S1, (b) Sample #S2, and (c) Sample #S3.

4) Experimental data analysis for quantitative corrosion assessment and comparison between soft coatings and hard coatings (Task 3 Subtask 3.2)

Figure 13 shows the monitored data after temperature compensation for all the three samples. It can be found from this figure that in soft coating, the monitored wavelength approaching stable

state roughly around 700 hours (29 days) for Sample #S1 and 1000 hours (42 days) for Sample #S2 and Sample #S3. Comparing this result to previous results from accelerated corrosion tests conducted on samples coated with hard coatings as seen in Figure 14, which normally required less than 4 days. It is obvious that the soft coating slowed down corrosion development more efficiently.

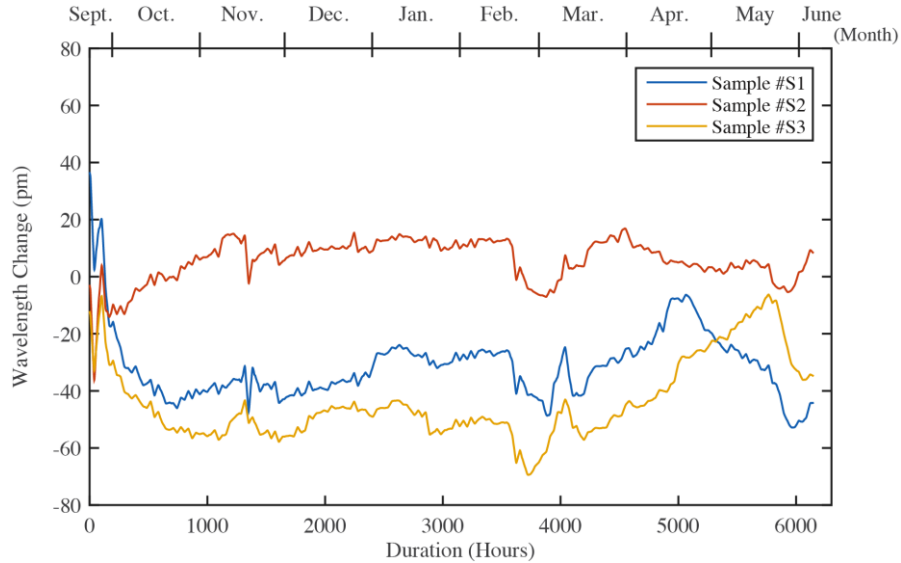


Figure 13. Bragg wavelength changes collected from FBG sensor with soft coating after eliminating temperature effect and de-noising.

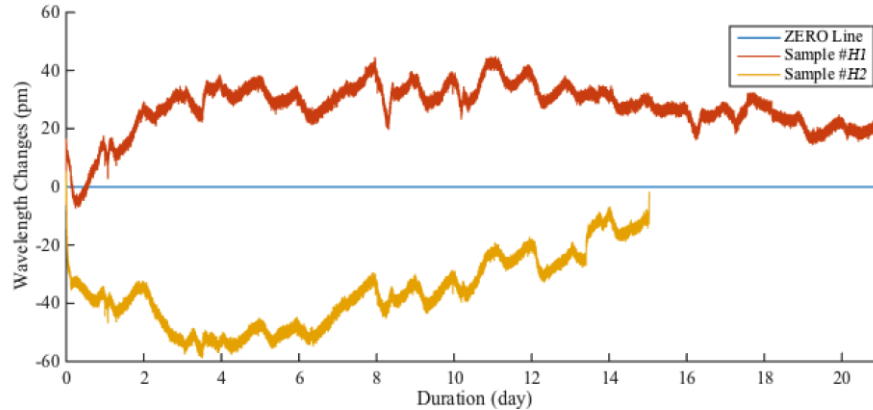


Figure 14. Bragg wavelength changes collected from accelerated corrosion test conducted on samples coated with hard coating.

Also, if the corrosion analysis for soft coating is analyzed based on the findings from the hard coatings as shown in Figure 14 (Sample #H1 was pitting corrosion and Sample #H2 was uniform corrosion), the curve pattern in Figure 13 indicated that Sample #S2 had a pitting corrosion on top of the embedded sensor because its wavelength change increased immediately after corrosion started and Sample #S1 and Sample #S3 would have a uniform corrosion propagation because their wavelength change decreased after corrosion started. However, the visual inspection results from Figures 10~12 did not support this assumption since as it can be seen from those figures, all samples showed pitting corrosion development instead of uniform corrosions beneath the soft coatings. This finding means that we cannot use the same assumptions as made for hard coating to

analyze the corrosion behavior of soft coatings. Systematic analysis of soft coatings need to be performed separately for corrosion analysis using embedded sensing systems.

The possible reason for wavelength change with soft coating having a different pattern even with the same type of corrosion pattern could be a result of very different bonding strength between soft and hard coatings. In a hard coating with high bonding strength, when a pitted corrosion occurs, only small portion of coating near the corroded area were detached from base material, resulting in concentrated stress and significant increase of wavelength from the embedded sensors.

On the other hand, soft coatings generally have less bonding adhesion at the coating interface comparing to hard coatings. When pitting corrosion occurred under soft coatings, it was more likely that a relatively larger portion of coating near the corroded area were detached from base material, which is known as a delamination. This phenomenon would first decrease the overall stress level around the embedded sensors, leading to a decrease in wavelength. With the corrosion progressing, it would gradually increase the amount of corrosion products which filled up the free space and increase the overall stress around the embedded sensors. As a result, the center wavelength of the embedded fiber optic sensor would have a decrease followed by an increase as observed in the monitored data. It's worth noticing that the soft coatings normally have lower porosity compared to hard coatings, so corrosion would develop much slower with application of soft coating when there were no external damages. Thus the wavelength increase was much slower when soft coating is applied. Under soft coating, the center wavelength of sensor embedded in Sample #S1 increased about 20 pm in 4 months as seen in Figure 13,; compared to 40pm changes of center wavelength of sensor embedded in Sample #H2 in 11 days under hard coating as in Figure 14.

This phenomenon could be further confirmed after cracks on top of sensors were intentionally made on each sample on Day 150 (February 20th, 2017) as shown in Figure 15. A decrease on center wavelengths of the embedded fiber optic sensors could be found on Day 150, followed by an increase after 10 days.. When crack occurred, there would be more coating delamination, leading to a decrease in center wavelengths of sensors. However, because the cracks broke the barrier between base material and outer environment, the corrosion of the base material would increase and corrosion products would start to fill up the free space beneath the soft coating. As a result, the wavelength of the embedded sensors would increase until the coating was penetrated. After coating penetrated by the corrosion products, the wavelength change curve decreased again. In the visual inspection result in Figure 12, it was clear that large portion of soft coatings were delaminated in Sample #S1 (middle part), Sample #S2 (right part), and Sample #S3 (bottom-right part). Clearly, the embedded fiber optic sensors successfully and effectively captured the entire corrosion progress of the steel materials coated soft coatings including the early stage of corrosion, coating delamination progressing, crack initiation, and coating breakage.

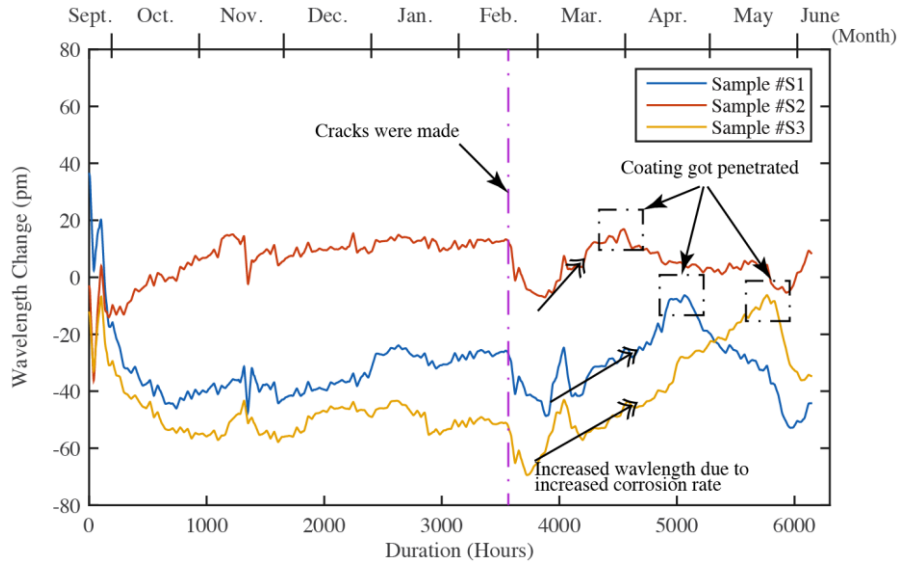


Figure 15. Bragg wavelength changes with detailed time tags marked

(c) Description of Problems/Challenges

The corrosion experiment for soft coating was a relatively long test (9 months) and the fiber optic sensors successfully survived the entire duration of corrosion monitoring procedure and they are still working perfectly for monitoring of the coating behavior after its breakage.

(d) Planned Activities for the Next Quarter

The planned activities for next quarter are listed as below:

- 1) Optimizing coating thickness design and coating samples with embedded sensors and perform corrosion tests on the samples (Task 2.5);
- 2) Localize corrosion locations on both hard coatings and soft coatings through embedded sensor network (Task 3.2);
- 3) Sensor networking and corrosion damage characterization (Task 3.2).